Semnan University

Progress in Physics of Applied Materials

journal homepage: https://ppam.semnan.ac.ir/

Fabrication of 3,4-dihydropyrimidin-2-(1H)-ones/thione compounds via $Cu_2V_2O_7$ nanocatalyst synthesized by solid state method

L. Kafi-Ahmadi[a*], Sh. Khademinia[b]

[a]*Department of Inorganic Chemistry, Faculty of Chemistry, Urmia University, Urmia, Iran.*
[b]*Department of Inorganic Chemistry, Faculty of Chemistry Semnan University, Semnan 35351-19111, Iran.*

ARTICLE INFO

Article history:
Received: 14 July 2022
Revised: 4 October 2022
Accepted: 18 October 2022

Keywords:
Copper pyrovanadate
Solid state
Nanomaterial
Catalyst
Biginelli

ABSTRACT

Synthesis of Cu2V2O7 nanoparticles was performed successfully using $Cu(NO_3)_2$ and V_2O_5 raw compounds in one step solid state method. $Cu_2V_2O_7$ nano powders were used as photocatalysts to remove pollutant dye under visible light irradiation. X-ray diffraction (XRD) technique was applied to characterize the crystal phase type of the as-prepared sample. The XRD results showed that the patterns had a main $Cu_2V_2O_7$ structure with a space group of C2/c. Field emission scanning electron microscopy (FESEM) images showed that the synthesized $Cu_2V_2O_7$ particles had mono-shaped sphere morphologies. The as-prepared $Cu_2V_2O_7$ nanomaterial exhibited high catalytic activity in multi-component reaction for the one-pot synthesis of heterocyclic compound 3,4-dihydropyrimidin-2(1H)-ones (DHPMs). Additionally, the nanocatalyst can be reused for several times without apparent loss of its catalytic activity, confirming it is a highly stable and reusable material for this reaction. It is found that the optimum values for catalyst amount, reaction time and temperature are 50 mg, 50 min and 90 ºC, respectively.

1. Introduction

Oxides and fluorites with common equation $A_2B_2O_7$ in which A may be a medium-large cation and B is an octahedrally facilitated and high oxidation state cation are numerous samples broadly examined for their excellent applications in technological fields [1,2]. Pyrochlore stage may be an imperfect structure of fluorite sort with common equation $A_2B_2O_6$ or $A_2B_2O_7$. Investigation on pyrochlore samples have been focused because of their use in catalysis [3, 4], gadgets [5], optics [6] and solid oxide fuel cell (SOFC) anode materials [7, 8]. There are three polymorphs for $Cu_2V_2O_7$ counting gamma, alpha, and beta-$Cu_2V_2O_7$. The two copper pyrovanadate crystal structures are n-type metal oxide semiconductors, that possess appropriate backhanded and coordinate optical bandgaps within the run of 1.8–2.1 eV. The $Cu_2V_2O_7$ has electrical, attractive, thermoelectric, electrochemical, and catalytic properties. Uncommon endeavors exist to investigate the application of metal vanadate as catalyst in the photocatalysis process and also, there are few published works available about the supercapacitor application. The Biginelli response, which was initially detailed by Biginelli in 1891 [9], could be a technique for the union of 3, 4-dihydropyrimidin-2-(1H)-one subordinates (DHPMs) in a one-step strategy. DHPMs compounds are as of now appeared organic exercises [10]. Some metal oxides have been introduced as nanocatalysts for the Biginelli processes that are explained in refs. [11-17]. Within the display ponder, the amalgamation of $Cu_2V_2O_7$ nanomaterial is detailed by solid state strategy. The application of the synthesized $Cu_2V_2O_7$ as catalyst in the reaction mixture was examined in Biginelli process. It was found that the synthesized $Cu_2V_2O_7$ sample had fabulous productivity for the blend of DHPMs.

2. Experimental

2.1. General remarks

The used compounds were of expository review, obtained from commercial sources, and utilized without assist decontamination. Stage recognizable pieces of proof were done on an X-ray powder diffractometer D5000 using CuK_α illumination. Hitachi FE-SEM S-4160 was utilized to consider the morphology of the obtained materials. The immaculateness of specimens was tested by thin layer chromatography (TLC) a glass plate coated with silica gel 60 F254 utilizing n-hexane/ethyl acetic acid derivation blend as portable stage. Thermo logical 9100 device was utilized to record the dissolving focuses of the DHPMs samples.

* Corresponding author. Tel.: +98-443255294
E-mail address: L.kafiahmadi@urmia.ac.ir

DOI: 10.22075/PPAM.2022.27811.1032

2.2. Solid state synthesis of $Cu_2V_2O_7$

$Cu_2V_2O_7$ is fabricated by mixing 0.2 g of $Cu(NO_3)_2.5H_2O$ (Mw = 211.62 g mol^{-1}) and 1.0 mmol of V_2O_5 (Mw = 197.87 g mol^{-1}) that were ground in a ceramic mortar to obtain a fine powder sample. The sample was transferred into a 25 mL ceramic crucible and to heated in a one step at 800 ºC for 6 h in a preheated furnace. The crucible was cooled down to the room temperature normally.

2.2. DHPMs synthesis in a catalytic rout

In a commonplace method, a blend of benzaldehyde (C_7H_6O), ethyl acetoacetate ($C_4H_8O_2$), and urea ($CO(NH_2)_2$ with the molar proportion of 1:1:1.2, individually, and certain sum of catalyst ($Cu_2V_2O_7$) were poured into a circular foot jar. The suspension was mixed at desired response temperature which was outlined by the plan master computer program. At the certain outlined time, the solid powder was isolated and washed with refined water to separate the unreacted crude materials. At that point, the obtained unrefined DHPM was broken down in ethanol to separate $Cu_2V_2O_7$ and crystallized at room temperature to get the immaculate DHPM. The test outlined strategy shown in table 1 was done by changing the response parameters simultaneously. The response abdicates for each outlined test were calculated by measuring the mmole division of the ultimate item.

3. Results and discussion

3.1. Characterization

The PXRD pattern of the as-fabricated $Cu_2V_2O_7$ sample is reported in figure 1. β-$Cu_2V_2O_7$ that is characterized by ziesite phase with 2:1 molecular ratio of CuO and V_2O_5, matched well with the JCPDS Card No: 01- 073-1032 with space group of C2/c. The cell factors of β-$Cu_2V_2O_7$ are a = 7.680 A˚ , b = 8.007 A˚ , c = 10.090 A˚ , and a = c = 90°, b = 110.45°. High purity of the sample with observing no other crystal phases is confirmed. This indicates that the synthesized β-$Cu_2V_2O_7$ is highly pure with the narrow diffraction peaks.

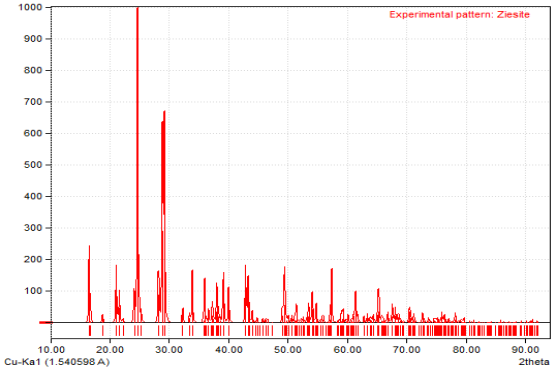

Fig. 1. XRPD pattern of $Cu_2V_2O_7$ nanomaterial.

3.2. Morphology analysis

Fig. 2 shows typical FESEM images of $Cu_2V_2O_7$. As can be seen from figure 2, the morphology of the sample is a sponge-like structure. Besides, it is clear that the particles formed the sponge structure are in the nanoscale size. It is found that the particle sizes are about 70-90 nm.

Table 1. Three-level full factorial design in Biginelli reaction.

t	catalyst	T	Y%
50	50	30	37
20	50	90	56
20	30	30	16
50	30	90	79
35	40	60	33
35	40	60	36
20	30	90	45
35	40	60	34
50	30	30	23
50	50	90	70
35	40	60	33
20	50	30	23
35	23	60	26
60	40	60	52
35	40	10	15
10	40	60	25
35	57	60	53
35	40	60	31
35	40	60	35
35	40	110	79

3.3. Obtaining optimum conditions by Experimental design method

Full factorial plan is utilized to get the ideal conditions within the Biginelli responses by mixing all of the components and their settings. To study the exploratory plan, reaction surface technique (RSM) is utilized by employing an observational demonstrate. The investigation of change Analysis of Variance (ANOVA) was utilized to check the ampleness of the connected demonstrate. For the reason, a few replicated experiments are required within the show. The objective of the display exploratory plan ponder is deciding the values of nanocatalyst, response time (t) and temperature (T) in which the most extreme response (Y (%)) is accomplished. All the likely combinations of the three variables related to the reaction values are displayed in table 1. All of the tests are done for two days haphazardly. Four reproduces at the center of the components are considered to approve the connected shown by ANOVA (Table 2). The low and high levels of the over said components were coded to -1 and +1, separately (Table 3). The observed information of the factorial plan was fitted to a straight reaction demonstrate. The connection between the three variables (catalyst, t and T) and the surrender of the Biginelli response, Y%, is appeared underneath based on the primary arrange show: R_1=+33.66+8.41A+5.00B+19.01C-1.62AB+3.38AC 2.37BC+2.06A^2+2.33B^2+5.12C^2 Table 2 shows the investigation of fluctuation for recommended first-order demonstrate. The information demonstrates that the p-value of the relapse is lower than 0.05. So, it reveals that the show is noteworthy at a high certainty level (95%) [38]. In addition, it is found that the p-value of need for fitting is more prominent than 0.05, affirming the

noteworthiness of the demonstrate. Furthermore, two parameters (R-square and adjusted–R-square) obtained by the ANOVA are utilized to precise the quality of fitting of the direct show condition. It was found that the esteem of variety fitting (R^2) is 0.98 showing a high degree of relationship between the reaction and the autonomous variables. Moreover, high importance of the proposed demonstrate was affirmed by the tall values of balanced relapse coefficient (R^2-adj = 0.96) and anticipated relapse coefficient (R^2-prd = 0.77). 2D and 3D reaction surface plots of Y% (utilizing condition (1) when the sum of temperature was kept up consistent at ideal esteem and the other two components were permitted to change) are presented in figure 5 to demonstrate the impacts within the said variables.

The above-mentioned exploratory plan technique in the present research was utilized to discover the ideal conditions for the Biginelli response with few number of tests instead of one-at-a-time strategy. With implying RSM strategy to analyze the strategy, it was observed that the parameters (catalyst, t and T) were free parameters. Their impacts on the process response (Y%) were portrayed and translated with the RSM strategy. The optimization results obtained by the total factorial plan appeared that the ideal condition for the blend of the DHPMs was 0.05 g of catalyst, 90 ºC response temperature, and 50 min response time (Table 1). The proper conditions were utilized for the blend of other subordinates. Schematic picture is displayed underneath to appears a outline of the Biginelli response pathway (Fig. 3).

3.4. Catalytic studies

Table 2. Analysis of variance for the suggested first-order model.

Source	Sum of Squares	df	Mean Square	F-value	p-value	
Block	74.12	2	37.06			
Model	6804.30	9	756.03	49.36	< 0.0001	significant
A-Time	958.72	1	958.72	62.60	< 0.0001	
B-Catalyst	344.50	1	344.50	22.49	0.0015	
C-temperature	4897.78	1	4897.78	319.78	< 0.0001	
AB	21.12	1	21.12	1.38	0.2740	
AC	91.12	1	91.12	5.95	0.0406	
BC	45.12	1	45.12	2.95	0.1244	
A^2	59.45	1	59.45	3.88	0.0843	
B^2	80.70	1	80.70	5.27	0.0508	
C^2	367.08	1	367.08	23.97	0.0012	
Residual	122.53	8	15.32			
Lack of Fit	109.53	5	21.91	5.06	0.1063	not significant
Pure Error	12.98	3	4.23			
Cor Total	7000.95	19				

*For more information about the table, read ref. [18-20].

Table 3 shows the test run and levels of the three components utilized within the test plan strategy. The central composite plan (CCD) is selected to demonstrate the proposed strategy depicted in table 3. The factors (catalyst (A) and t (B) and, T (C)) are given in coded shapes.

The impact of the three autonomous components on the proposed reaction displayed by exploratory plan strategy was considered by RSM. Fig. 4 refers to the 2D and 3D plots correspond to the interaction of AB, AC and BC. The semi-curvature of the plots shows the interaction between the factors. The information displayed within the figure reveal that the DHPMs generation rate is upgraded when the catalyst sum and response time are expanded at a certain reaction temperature. This can be because of the accessibility of tall surface zone of the catalyst for the crude compounds to deliver the targets.

The typical residuals plot and anticipated versus the exploratory generation effectiveness plots are presented in figure 5. The information displayed within the figure shows a great agreement between the anticipated and exploratory effectiveness and speaks to the ampleness and centrality of the show. In addition, the typical plots of the inside studentized residuals versus likelihood and anticipated versus actual data are presented within the figure. As it is clear in this figure, the information shows up on a slanted slant line illustrating that there is no significant dispersal.

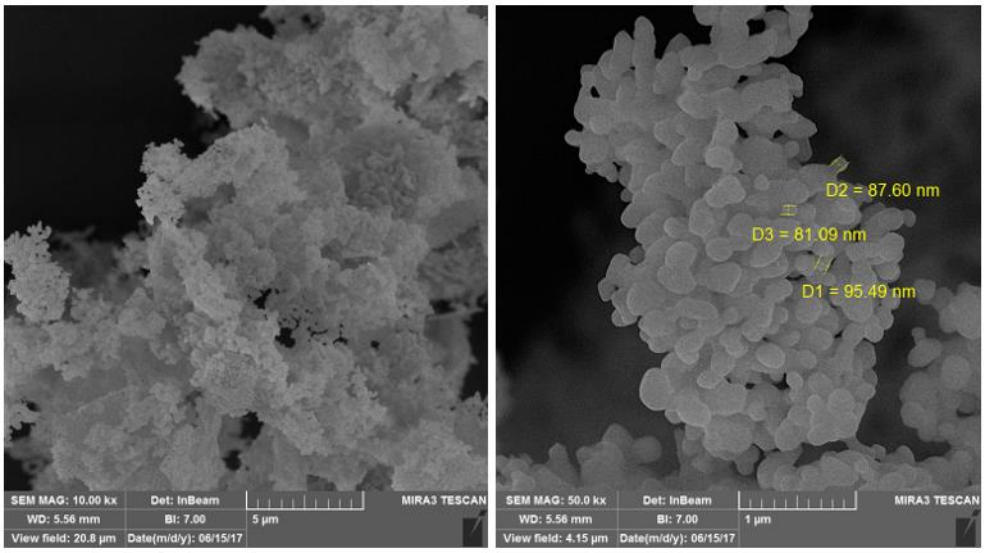

Fig. 2. FESEM images of $Cu_2V_2O_7$ nanomaterial.

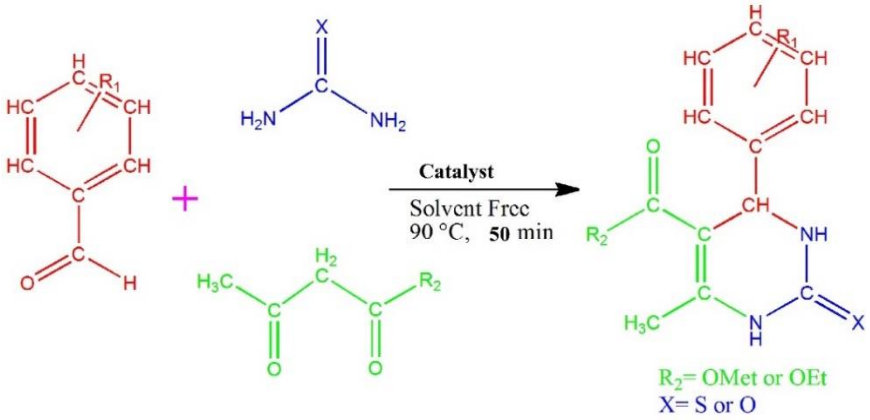

Fig. 3. Catalytic reaction pathway for the fabrication of DHPM compounds.

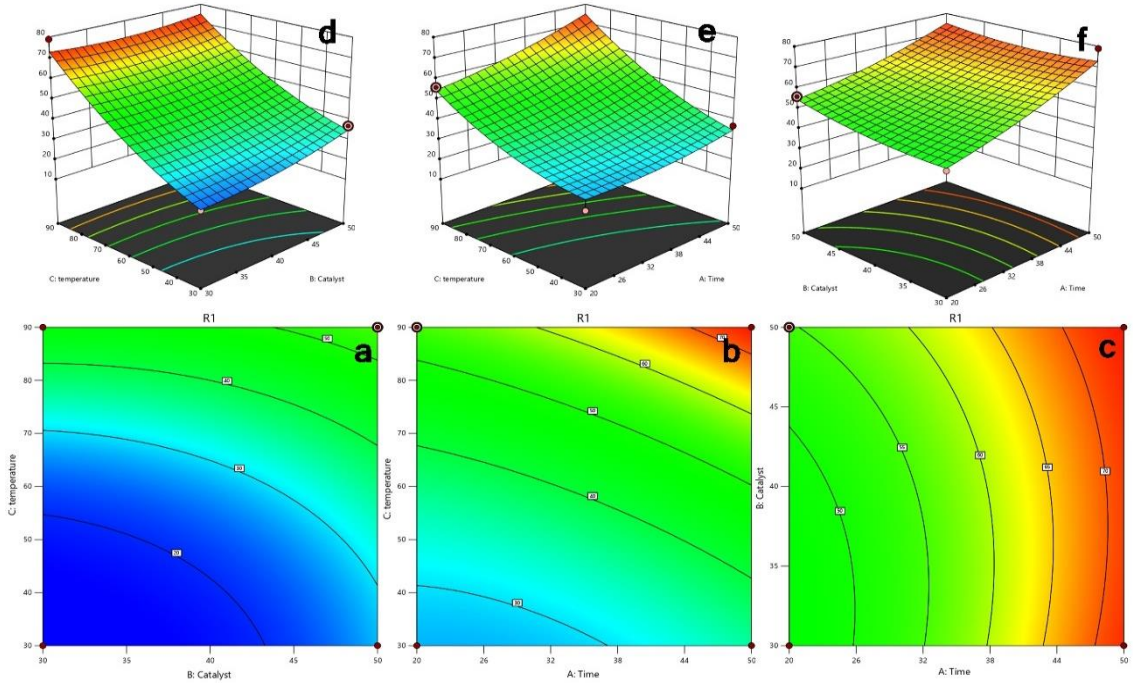

Fig. 4. 2D and 3D surface plots of the production of DHPM compounds.

Table 3. Experimental range and levels of the independent variables in CCD model.

Factor	Name	Minimum	Maximum
A	Time	10.00	60.00
B	Catalyst	23.00	57.00
C	temperature	10.00	110.00

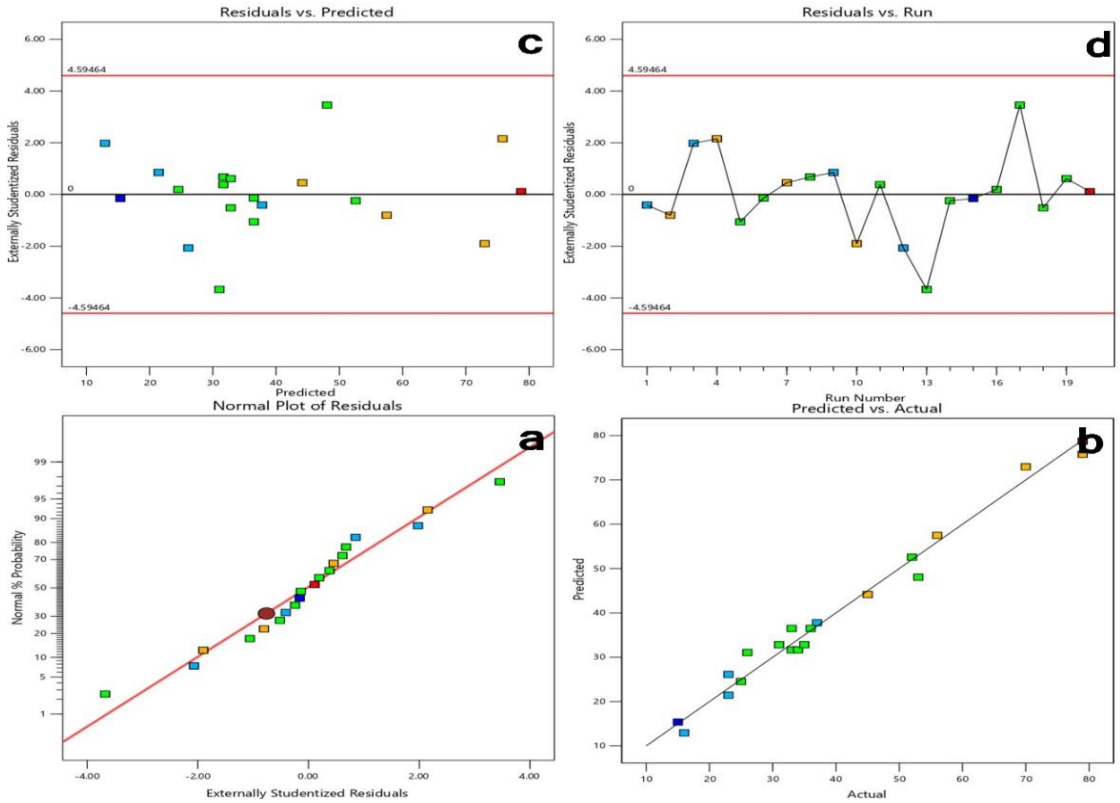

Fig. 5. a) normal plot of residuals, b) predicted versus actual, c) experimentally studentized residuals versus predicted and d) experimentally studentized residuals versus run number plots for the Biginelli reaction.

The ideal values of the three components (utilizing in run choice for the variables and greatest esteem for reaction (R)) obtained by RSM are displayed in figure 6. It is found that the ideal values for catalyst sum, response time, and temperature are 50 mg, 50 min, and 90 ºC, individually.

Box-Cox plot (Fig. 7a) guides us almost the choice of a fitting control change of yield factors in the event that required. Cook's separate plot reveals data with respect to change in relapse due to the exclusion of any exploratory run from watched information and is recommended for no location of an exception. The use esteem of a point proportionate to one indicates that point accurately fits the recorded data (Figure 7b) and controls the chosen demonstrate. All the used values were found in acceptable limits. DFFITS vs Run charts (Figure 7c) clarify the impacts of each plan point on the expected esteem. DFBETAS vs Run chart decides the effect of each planning point on the relapse coefficients (Figure 7d). The irritation plots displayed in figure 7e illustrate the comparative impact of all the variables at a specific point within the plan space. This plot makes a difference in recognizing the factor that has the foremost impact on the reaction rate. A noteworthy soak slant or ebb and flow of components A, B, and C appears that the blend reaction rate is touchy for all components considered in this case. The higher slant of calculating B (sum of catalyst) demonstrates its high affectability to the reaction.

Table 4 shows a comparative ponder on the catalytic execution of $Cu_2V_2O_7$. The information demonstrate that the finest union surrender was accomplished when benzaldehyde, urea and ethyl acetic acid derivation were utilized as the DHPM starting materials. Be that as it may, the information reveals that the surrender esteem of the Biginelli responses was least when methyl acetic acid derivation was utilized as starting materials.

Table 4. Comparative study on the catalytic performance of $Cu_2V_2O_7$ nanomaterial.

R_1	R_2	R_3	Y%
C_7H_6O	$C_4H_8O_2$	$CO(NH_2)_2$	72
C_7H_6O	$C_3H_6O_2$	$CO(NH_2)_2$	70
C_7H_6O	$C_3H_6O_2$	$CS(NH_2)_2$	76
C_7H_6O	$C_4H_8O_2$	$CS(NH_2)_2$	73

Table 5 presents the catalytic performance of the as-fabricated $Cu_2V_2O_7$ nanomaterial at the optimized conditions using different raw materials derivatives associated with the obtained melting points of the synthesized DHPMs compounds.

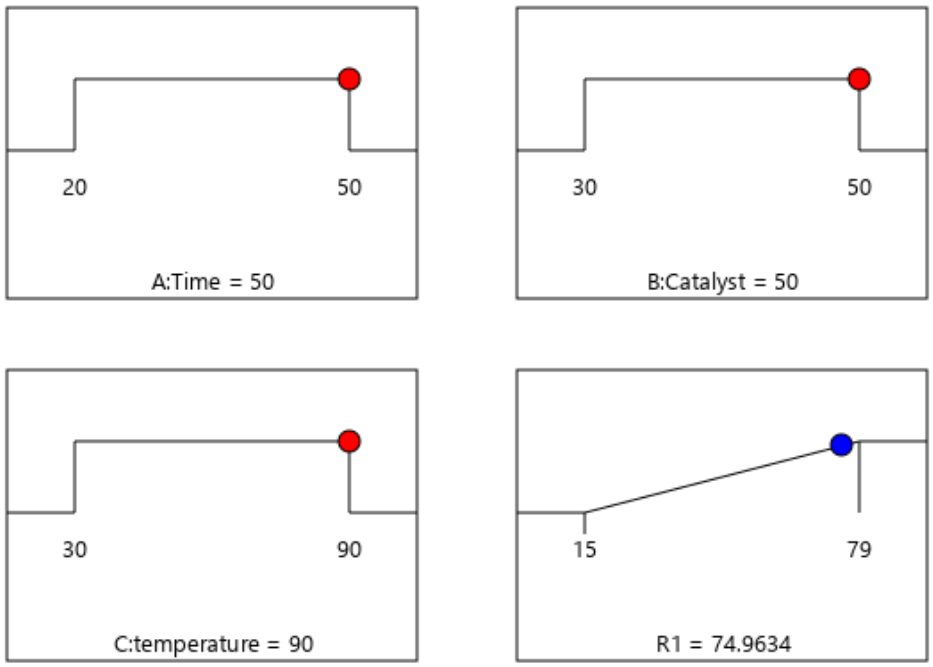

Fig. 6. Optimum amounts of the parameters in the present Biginelli reaction.

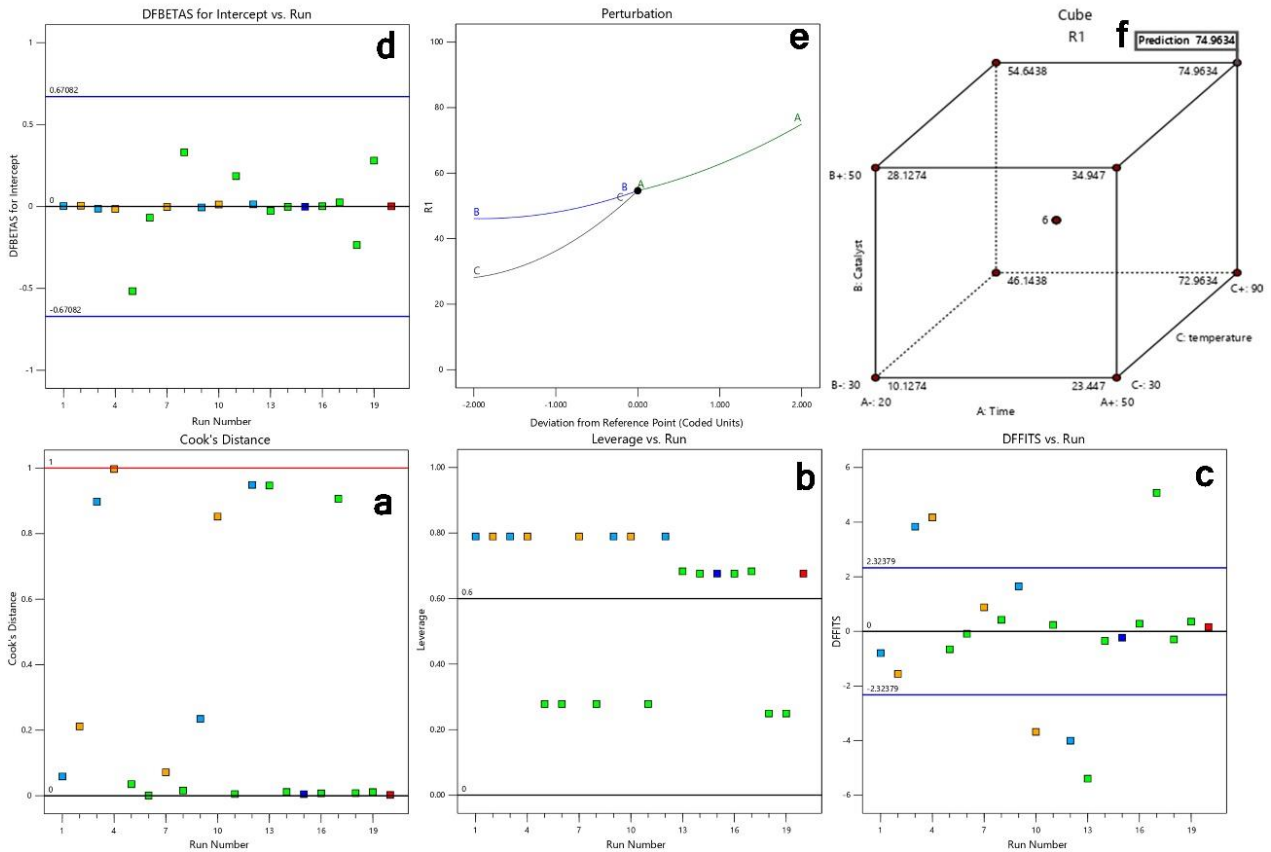

Fig. 7. a) Diagnostic Plots obtained by the Box-Behnken Design showing the interactions among factors, b) leverage versus run number, c) DFFITS versus Run number, d) DFBETAS versus Run number, e) Perturbation plot of operational parameters obtained through RSM and f) Cube representation showing the standard error of design and interaction effect of factors.

Table 5. Catalytic activity of $Cu_2V_2O_7$ at the optimized conditions using different raw materials derivatives.

R_1	R_2	Y%	Found Melting Point (°C)
H	OEt	77	197-199
4-Cl	OEt	72	208-210
2-Cl	OEt	70	214-217
4-Br	OEt	66	211-214
3-NO_2	OEt	80	224-226
2-OMe	OEt	60	261-263
3-OMe	OEt	31	256-258
3-OH	OEt	44	165-167
4-OH	OEt	51	252-255
H	OMet	73	203-205
4-Cl	OMet	69	201-203
2-Cl	OMet	75	226-229
4-Br	OMet	46	238-241
3-NO_2	OMet	78	277-280
2-OMe	OMet	12	282-285
3-OMe	OMet	42	191-193
4-OH	OMet	21	238-240

4. Conclusion

The present study detailed the solid state method of Cu2V2O7 material preparation. PXRD information revealed that Cu2V2O7 was crystallized well in monoclinic precious stone framework with C2/c space group. FESEM images showed that the morphology of the synthesized samples was wipe. The gotten nanomaterials were utilized as tall proficient nanocatalyst for the union of DHPMs. The ideal conditions were obtained by test plan strategy. It was found that the ideal conditions obtained by RSM examination were 50 mg of catalyst, 90 °C temperature and 50 min time. The blend surrender at the ideal condition was 74%.

References

[1] J.B. Thomson, A.R. Armstrong, P.G. Bruce, A New Class of Pyrochlore Solid Solution Formed by Chemical Intercalation of Oxygen, J. Solid State Chem. 148 (1999) 56-62.

[2] H. Kishimoto, T. Omata, S. Otsuka-Yao-Matsuo, K. Ueda, Crystal structure of metastable κ-CeZrO4 phase possessing an ordered arrangement of Ce and Zr ions, J. Alloys and Comp. 312 (2000) 94-103.

[3] D.J. Haynes, D.A. Berry, D. Shekhawat, J. J. Spivey, Catalytic partial oxidation of a diesel surrogate fuel using an Ru-substituted pyrochlore, Catal. Today. 136 (2008) 206-213.

[4] R. Kieffer, M. Fujiwara, L. Udron, Y. Souma, Hydrogenation of CO and CO2 toward methanol, alcohols and hydrocarbons on promoted copper-rare earth oxides catalysts, Catal. Today. 36 (1997)15-24.

[5] K. Matsuhira, M. Wakeshima, Y. Hinatsu, S. Takagi, Metal–Insulator Transitions in Pyrochlore Oxides Ln2Ir2O7, J. Phys. Soc. Jap. 80 (2011) 094701.

[6] M.G. Brik, A.M. Srivastava, N.M. Avram, Comparativ analysis of crystal field effect and optical spectroscopy of six-coordinated Mn4+ ion in the Y2T2O7 and Y2Sn2O7 pyrochlores, Optical Mater., 33 (2011) 1671-1676.

[7] K.A. Ross, L.R. Yaraskavitch, M. Laver, J.S. Gardner, J.A. Quilliam, S. Meng, J.B. Kycia, D.K. Singh, T. Proffen, H.A. Dabkowska, B.D. Gaulin, Dimensional evolution of spin correlations in the magnetic pyrochlore Yb2Ti2O7, Physical Review B., 84 (2011) 174442.

[8] J.K. Gill, O.P. Pandey, K. Singh, Ionic conductivity, structural and thermal properties of pure and Sr2+ doped Y2Ti2O7 pyrochlores for SOFC. Solid State Sci., 13 (2011) 1960-1966.

[9] P. Biginelli, Ueber Aldehyduramide des Acetessigäthers, Ber. Dtsch. Chem. Ges., 24 (1891)1317-1319.

[10] K. Singh, D. Arora, S., Singh, Genesis of Dihydropyrimidinoneψ Calcium Channel Blockers: Recent Progress in Structure-Activity Relationships and Other Effects, Mini Rev. Med. Chem., 9 (2009) 95-106.

[11] K. Kouachi, G. Lafaye, S. Pronier, L. Bennini, S. Menad Mo/γ-Al2O3 catalysts for the Biginelli reaction. Effect of Mo loading, J. Mol. Catal. A: Chem., 395 (2014) 210-216.

[12] F. Tamaddon, S. Moradi, Controllable selectivity in Biginelli and Hantzsch reactions using nano ZnO as a structure base catalyst, J. Mol. Catal. A: Chem., 370 (2013) 117-122.
[13] S. Samantaray, B.G. Mishra, Combustion synthesis, characterization and catalytic application of MoO3–ZrO2 nanocomposite oxide towards one pot synthesis of octahydroquinazolinones, J. Mol. Catal. A: Chem., 339 (2011) 92-98.
[14] J. Safari, S.G. Ravandi, MnO2–MWCNT nanocomposites as efficient catalyst in the synthesis of Biginelli-type compounds under microwave radiation, J. Mol Catal. A: Chem., 373 (2013) 72-77.
[15] H.R. Memarain, M. Ranjbar, Substituent effect in photocatalytic oxidation of 2-oxo-1,2,3,4-tetrahydropyrimidines using TiO2 nanoparticles, J. Mol. Catal. A: Chem., 356 (2012) 46-52.
[16] J. Lal, M. Sharma, S. Gupta, P. Parashar, P. Sahu Agarwal D.D., Hydrotalcite: A novel and reusable solid catalyst for one-pot synthesis of 3, 4-dihydropyrimidinones and mechanistic study under solvent free conditions, J. Mol. Catal. A: Chem., 352 (2012) 31-37.
[17] S. Khademinia, M. Behzad, H.S. Jahromi, Solid state synthesis, characterization, optica properties and cooperative catalytic performance of bismuth vanadate nanocatalyst for Biginelli reactions, RSC Adv., 5 (2015) 24313.
[18] Box GEP, Draper NR Empirical Model-Building and Response Surfaces, Wiley, New York, 1987.
[19] S. Masaya, S. Masaki, Y. Ito, An Enantioselective Two-Component Catalyst System: Rh–Pd-Catalyzed Allylic Alkylation of Activated Nitriles, J. Amer. Chem. Soc. 118 (1996) 3309-3310.
[20] Y.F. Cai, H.M. Yang, L. Li, K.Z. Jiang, G.Q. Lai, J.X. Jiang, L.W. Xu Cooperative and Enantioselective NbCl5/Primary Amine Catalyzed Biginelli Reaction, Eur. J. Org. Chem. (2010) 4986-4990.